IEEE Access
Multidisciplinary | Rapid Review | Open Access Journal

Received June 4, 2020, accepted June 21, 2020, date of publication June 30, 2020, date of current version July 20, 2020.

Digital Object Identifier 10.1109/ACCESS.2020.3006030

An Improved Empirical Mode Decomposition Based on Adaptive Weighted Rational Quartic Spline for Rolling Bearing Fault Diagnosis

XUERONG YE[1], (Senior Member, IEEE), YIFAN HU[1], JUNXIAN SHEN[2], RUI FENG[1], AND GUOFU ZHAI[1], (Member, IEEE)

[1]School of Electrical Engineering and Automation, Harbin Institute of Technology, Harbin 150001, China
[2]College of Aerospace and Civil engineering, Harbin Engineering University, Harbin 150001, China

Corresponding author: Yifan Hu (yifanhu_123@163.com)

This work was supported in part by the National Key Research and Development Program of China under Grant 2017YFB1300800, and in part by the National Natural Science Foundation of China under Grant 61671172.

ABSTRACT As a powerful time-frequency signal analysis technique, empirical mode decomposition (EMD) has been commonly applied in fault diagnosis. However, the cubic spline-curve often causes outstanding over and undershoot problem, which significantly limits the performance of conventional EMD. To address this problem, an improved EMD (I-EMD) based on adaptive weighted rational quartic spline is proposed. Firstly, the original cubic spline interpolation in conventional EMD is replaced with the weighted rational quartic spline interpolation (WRQSI) which has two adjustable shape control parameters. Secondly, a novel parameter selection criterion termed envelope characteristic frequency ratio (ECFR) is designed to guide the construction of the optimal local envelope. And simulation analysis proved that ECFR is not only sensitive to the characteristic information but also robust to the weak noise and sudden impulses. Subsequently, the optimal shape control parameter can be searched by grasshopper optimization algorithm (GOA) using the maximum ECFR as the objective function. Then the sensitive modes selected via weighted Kurtosis index are employed for further Hilbert envelope spectrum analysis. Finally, two case studies on rolling bearing fault diagnosis are constructed to verify the rationality and effectiveness of the I-EMD method. The results show that I-EMD method can evidently solve the over and undershoot problem and restrain the mode mixing phenomenon. Moreover, I-EMD also performs better fault feature extraction ability under the same conditions compared with EMD, VMD and CEEMDAN. So it is expected that I-EMD will serve as a potential improvement for signal processing, fault feature extraction and fault diagnosis.

INDEX TERMS Vibration signal processing, fault diagnosis, weighted rational quartic spline, improved EMD, envelope characteristic frequency ratio, parameter adaptive optimization.

I. INTRODUCTION

As a vital rotating machinery component, rolling bearings are widely used in large and complex mechanical systems of industries including aerospace, vehicles, ships and other fields. However, rolling bearings usually serve under adverse working conditions, which is prone to occur various categories of failure. At the same time, the failure often directly influences the operational condition of the whole mechanical system [1]–[5]. Therefore, condition monitoring and fault diagnosis techniques of rolling bearings in the early stage are very critical to guarantee reliability and safety. Vibration signal processing-based method has been a most effective fault diagnosis technique due to the definite relationship between the rolling bearing health conditions and the collected vibration signals. Hence, the fault feature information can directly reflect the performance and health conditions of rolling bearings [6]–[9].

In addition to the simple time or frequency-domain methods, wavelet transform (WT) [10], [11] and wavelet packet transform (WPT) [12], [13] have also been developed. However, the proper wavelet basis function of WT and WPT needs to be established in advance, so these two signal processing methods are not completely self-adaptive [5], [14].

The associate editor coordinating the review of this manuscript and approving it for publication was Ming Luo.

After that, empirical mode decomposition (EMD) was proposed as a completely self-adaptive signal analysis technique in 1998 by Huang et al, which can decompose the complex non-stationary signals into a series of intrinsic mode functions (IMF) [15]. Gai and Hu [16] realized the numerical recognition of bearing wear degree based on EMD-SVD and FNN. Ben *et al.* [17] calculated the energy entropy of the key IMFs as the learning samples of artificial neural network (ANN), which can identify different fault types of rolling bearings. However, some inherent problems in the conventional EMD such as mode mixing exactly limits its decomposition performance [18]. Therefore, many optimized and improved strategies on EMD have been continuously studied and applied. For noise-assisted signal analysis techniques, Xiang and Zhong [19] proposed a diagnosis scheme based on fast ensemble EMD (EEMD) and random decrement technique (RDT) to extract the explicit fault features of rotating machinery. Yang *et al.* [20] realized the adaptive diagnosis for bearings with unknown faults based on EEMD and stochastic resonance (SR). Cheng *et al.* [21] designed an improved CEEMDAN algorithm for vibration signal processing and fault detection of rolling bearings. Although the above-mentioned methods have already achieved gratifying results in the application, if used improperly, there are also some negative impacts such as the pre-added Gauss white noise can't be eliminated entirely, which will affect the decomposition accuracy. Besides, as an improvement of EMD, some variational mode decomposition (VMD) based strategies are also widely applied in fault diagnosis of rotating machinery [22]–[24]. Meanwhile, many researchers believe that a major and fundamental reason of mode mixing in conventional EMD is the over and undershoot problem caused by the cubic spline-curve [25], [26], so they still continue to optimize and improve the sifting process of EMD. Xia and Zhang et al modified the local extrema by designing a doubly iterative EMD to improve the decomposition performance [27]. In addition, various effective interpolation methods, such as trigonometric interpolation [28], B-spline interpolation [29] and cubic Hermite interpolation [30] have also been studied and applied to replace the cubic spine interpolation. However, in [28]–[30], the shape of interpolation is uncontrollable, which can't adaptively adjust the changeable curve in the dynamic sifting process. By adding a shape control parameter, Li *et al.* [31] proposed a cubic trigonometric B-spline interpolation based EMD method, but the flexible shape parameter in this paper was adjusted by experience and constant trying, which will limit the performance of the improved method. Consequently, the adaptive and accurate selection of shape parameter is another critical problem for improving the EMD method, because if the parameter itself is not enough suitable, it will lead an absurd decomposition result. Li *et al.* [32] developed a novel improved EMD method based on rational Hermite interpolation, and the optimal shape parameter is obtained by analyzing the geometric meaning of envelope curve. Guo and Deng [33] constructed the envelope curve with a new rational spline interpolation method, and the envelope curve length as well as frequency bandwidth is employed as the parameter selection criterion. In [32], [33], the rational Hermite and rational spline interpolation methods are employed to construct the envelope curves successfully. Meanwhile, it has been exactly proved that spline-based envelope curve is more smooth and stable than the Hermite-based envelope curve [33]. Inspired by the previous research, a novel interpolation method termed weighted rational quartic spline interpolation (WRQSI) is designed in this paper to construct more flexible envelope curves. Compared with the previous interpolation methods, WRQSI has the following two advantages: 1) WRQSI is C2 continuous, and it has good shape-preserving and approximation properties; 2) Besides the shape control parameters, WRQSI also introduces a weighted coefficient, which can properly solve the problem that no suitable envelope curves will be obtained due to the lack of flexibility under some certain conditions. On the other hand, the shape control parameter selection criterion proposed in [32], [33] totally concentrate on the geometrical form and physical meaning of the envelope curve itself. This kind of selection criterion is exactly meaningful, however, the high-quality IMF components which conclude abundant and explicit fault feature information are also desirable to be obtained in the engineering practice. Thus, inspired by the redefined signal to noise ratio (SNR) in [34], a novel envelope characteristic frequency ratio (ECFR) is proposed to select the optimal shape parameter and obtain the more satisfactory IMF components in this paper. ECFR represents the proportion of fault characteristic frequency information in the whole signal, which is pretty sensitive to the impact properties. When the periodic impact properties become more obvious in the vibration signal, the ECFR will be larger, which denotes a better decomposition performance, vice versa. Considering the excellent global optimization performance compared with other search algorithms, grasshopper optimization algorithm (GOA) [35], [36] which was proposed in 2017 is employed to search the optimal shape parameter in this paper.

The remaining sections of the paper is outlined as follows. The limitation of conventional EMD is clarified in Section II. The weighted rational quartic spline interpolation, the optimal parameter selection criterion termed ECFR and its superior properties, the basic algorithm of GOA are introduced in section III, and then the I-EMD is proposed. In section IV, two cases on rolling bearing fault diagnosis and the corresponding comparative analysis are presented to verify the proposed method. Finally, Section V concludes the whole paper and reiterates the highlights.

II. THE LIMATATION OF CONVENTIONAL EMD ALGORITHM

From the detailed description in [15], we can conclude that the core idea of EMD algorithm is subtracting the local mean iteratively to obtain the IMFs. It should be noted that the local mean is totally determined and generated by the upper and lower envelope curves. Hence, the proper construction

of envelope curve is very essential to obtain a satisfactory decomposition result. However, the cubic spline-envelope curve in conventional EMD will cause outstanding over and undershoot problems which are denoted by arrows in Fig. 1. This over and undershoot phenomenon is regarded as the inherent errors, it can further transfer into the whole sifting process when calculating the local mean, which eventually distort the physical meaning of IMF components and significantly influence the decomposition results [29]. The lack of flexibility in cubic spline-envelope curve is the exact reason for causing the over and undershoot problems [32]. Therefore, more flexible and accurate interpolation methods are desirable to be developed to improve the conventional EMD, which motivates the following research of this paper.

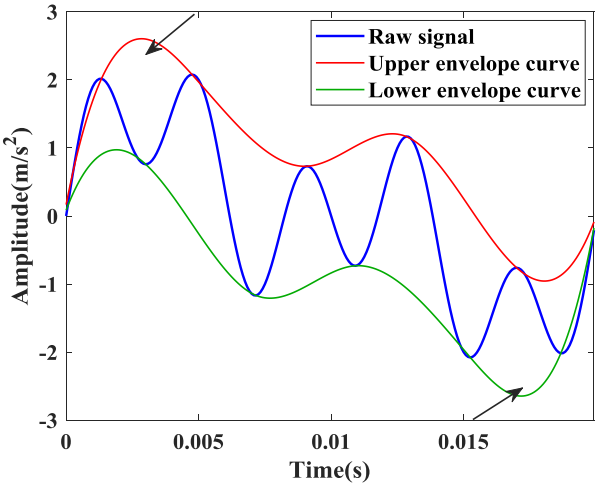

FIGURE 1. The over and undershoot problem of the cubic spline-curve.

III. THE IMPLEMENTATION OF IMPROVED EMD ALGORITHM

In this section, the weighted rational quartic spline interpolation for replacement is introduced firstly. Based on this, the adaptive optimized weighted rational quartic spline based EMD method is designed. The main thought of this optimized method is to obtain the optimum mode by searching for the optimal shape control parameters α and β, which includes two essential points: 1) The construction of optimal parameter selection criterion, and 2) Parameter optimization by GOA. The two points are introduced prior to the proposed I-EMD method.

A. A NEW INTERPOLATION METHOD: WEIGHTED RATIONAL QUARTIC SPLINE INTERPOLATION

A novel interpolation method termed weighted rational quartic spline interpolation is designed in this subsection to construct more flexible envelope curves. This interpolation function is C2 continuous, and it has good shape-preserving and approximation properties, which can alter the splines shape under different conditions through changing the shape parameters.

For a given $\{(t_i, g_i, d_i), i = 0, 1, \ldots, n\}$, g_i, d_i represents the function and derivative value of $g(t)$ at t_i, and $a = t_0 < t_1 < \cdots < t_n = b$, $l_i = t_{i+1} - t_i$, $\theta = (t - t_i)/l_i$, $\Delta_i = (g_{i+1} - g_i)/l_i$ are defined. $\alpha > 0, \beta > 0$ represents the shape control parameters. Now, the interpolation basis functions for fitting the envelope curve can be constructed as follows:

$$R(t) = \mu R^*(t) + (1-\mu)R_*(t) = \frac{r_i(t)}{s_i(t)}, \quad i = 0, 1, \ldots, n-2 \tag{1}$$

$$\begin{aligned} r_i(t) &= (1-\theta)^4\alpha_i g_i + \theta(1-\theta)^3 U_i + \theta^2(1-\theta)^2 V_i \\ &\quad + \theta^3(1-\theta)W_i + \theta^4\beta_i g_{i+1} \\ s_i(t) &= (1-\theta)\alpha_i + \theta\beta_i \end{aligned} \tag{2}$$

$$\begin{aligned} U_i &= (\mu\alpha_i + 2\alpha_i + \beta_i)g_i + \mu\alpha_i l_i d_i + (1-\mu)\alpha_i g_{i+1} \\ W_i &= (\alpha_i + 3\beta_i)g_{i+1} - \mu\beta_i l_i d_{i+1} - (1-\mu)\beta_i l_i \Delta_{i+1} \end{aligned} \tag{3}$$

where μ denotes the weighted coefficient, and $0 < \mu < 1$ is defined.

And the basis function $R(t)$ also satisfy the following relationships

$$R(t_i) = g_i, R'(t_i) = \mu d_i + (1-\mu)\Delta_i, i = 0, 1, \ldots, n \tag{4}$$

Further, when the following equation is assumed:

$$R''(t_i+) = R''(t_i-), \quad i = 1, 2, \ldots, n-1 \tag{5}$$

where t_i+ and t_i- represent the right and left limits of t_i, respectively.

The restraint condition of C2 continuity is expressed as (6):

$$\begin{aligned} &l_i^2\alpha_i[V_{i-1} - 3\alpha_{i-1}g_i - 3\beta_{i-1}g_i + \mu\alpha_{i-1}l_{i-1}d_i \\ &\quad + 2\mu\beta_{i-1}l_{i-1}d_i + (1-\mu)\alpha_{i-1}l_{i-1}\Delta_i + 2(1-\mu)\beta_{i-1}l_{i-1}d_i] \\ &\quad = l_{i-1}^2\beta_{i-1}[V_i - \alpha_i g_i - 2\beta_i g_i - 2\mu\alpha_i g_i - \mu\beta_i g_i - 2\mu\alpha_i l_i d_i \\ &\quad - \mu\beta_i l_i d_i - 2(1-\mu)\alpha_i g_{i+1} - (1-\mu)\beta_i g_{i+1}], \\ &\quad i = 1, 2, \ldots, n-2 \end{aligned} \tag{6}$$

As is described, the shape parameters α and β can independently influence the shape of envelope curve, while the weighted coefficient μ only jointly affect it by the form of $\mu\alpha, \mu\beta, (1-\mu)\alpha$ and $(1-\mu)\beta$. That is to say, if the μ is given in advance, once the optimal combination of shape control parameters α and β are obtained by the optimization, the $\mu\alpha, \mu\beta, \mu(1-\alpha)$ and $\mu(1-\beta)$ are also optimal. Hence, we just consider the optimization of α and β, while $\mu = 0.8$ is assigned in advance.

Fig. 2 displays the weighted rational quartic spline-based envelope curves with different shape parameters. Obviously, the over and undershoot problem is effectively restrained compared with cubic spline curve shown in Fig. 1. We can also see that the shape of envelope curve changes with different α and β, so the proper shape control parameters will bring the most satisfactory decomposition results. Hence, the shape parameter optimization process is very crucial to the improved EMD method.

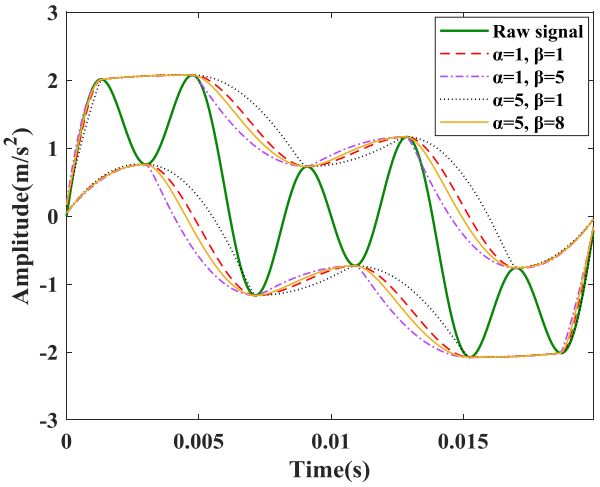

FIGURE 2. The weighted rational quartic spline-based envelope curves with different shape parameters.

B. THE CONSTRUCTION OF PARAMETER SELECTION CRITERION: ECFR

1) DEFINITION AND CALCULATION OF ECFR

The Hilbert demodulation analysis is a powerful and effective method to detect and diagnose the local fault of rolling bearings. An envelope signal by Hilbert transform can be considered as the combination of the valuable fault characteristic frequency information and some other interference components. ECFR represents the proportion of fault characteristic frequency information in the whole envelope signal, when the envelope signal contains more fault feature information associated with the impact properties, the ECFR value will be larger, vice versa. Thus, we establish the ECFR in this subsection to quantify the quality of the IMF components by comparing the proportion of fault feature information they contained, and then determine the optimal shape control parameter. For a vibration signal $X(t)$, the Hilbert transform is expressed as (7):

$$\tilde{X}(t) = \frac{1}{\pi} \int_{-\infty}^{\infty} \frac{X(\tau)}{t-\tau} d\tau \tag{7}$$

The analytic signal is obtained as (8):

$$Z(t) = X(t) + j\tilde{X}(t) = H(t)e^{j\omega(t)} \tag{8}$$

The envelope signal $H(t)$, phase modulation signal $\omega(t)$ can be calculated as (9) and (10), respectively:

$$H(t) = \sqrt{X^2(t) + \tilde{X}^2(t)} \tag{9}$$

$$\omega(t) = \arctan \frac{\tilde{X}(t)}{X(t)} \tag{10}$$

Subsequently, we can easily obtain the characteristic frequencies associated with all fault categories through Hilbert transform and FFT, so the ECFR is expressed as (11):

$$ECFR = \frac{\sum_{i=1}^{M} \sum_{j=1}^{N} E_n(f_{ij})}{E_n(A)} \tag{11}$$

where $E_n(f_{ij})$ represents the energy of the *ith* harmonic and *jth* type of characteristic frequency which we focus on, M and N denotes the number of the harmonic components and the characteristic types we select, respectively, $E(A)$ is the energy of the whole envelope signal. The localized defects emerged on the bearings will cause the transient impacts. Since the proposed ECFR is defined based on the Hilbert transform, so the high frequency components in the obtained IMFs will be demodulated to the low frequency. Therefore, the whole envelope signal, the fault characteristic frequency components and their harmonics are all analyzed within 1000Hz in this paper. As an effective parameter selection criterion, ECFR is not only sensitive to the characteristic information but also robust to the weak noise and sudden impulses. Simulation analysis is conducted in the next two subsections to illustrate its superior properties.

2) SENSITIVENESS TO THE PERIODIC IMPULSES

A mathematical model of bearing with localized defect [37] expressed as (12) is employed in this subsection to demonstrate ECFR is pretty sensitive to the periodic impulses as well as the fault characteristic information. Meanwhile, the Kurtosis index is also calculated for comparison.

$$\begin{cases} x(t) = \sum_{i=1}^{L} A_i s(t - iT - \tau_i) + \omega(t) \\ A_i = A_0 \cos(2\pi f_r t + \varphi) + C_A \\ s(t) = \exp(-Bt) \sin(2\pi f_n t + \varphi_\omega) \end{cases} \tag{12}$$

where $x(t)$ denotes the simulated vibration signal, L denotes the number of fault impulse, T is the impulse repetition period, τ_i is the random slippage of roller, $\omega(t)$ denotes the white Gaussian noise (WGN), A_i is the modulation signal, and $s(t)$ represents a discrete oscillation impulse signal. And in this case, the SNR of WGN is -1dB, the natural frequency $f_n = 3000$Hz, the inner race fault frequency $f_i = 123$Hz, the rotation frequency $f_r = 33$Hz, and the data points is 8192.

Fig. 3 (a) and (c) displayed the original simulation waveform with 1° and 30° random slippage of roller τ_i, respectively, and (b), (d) represent their envelope spectra. A smaller random slippage of roller τ_i indicates more obvious harmonic characteristic information and stronger periodic impulses. As shown in (b) and (d), the ECFR value reduces obviously when the periodic impulses is weakened by the increase of random slippage, while the Kurtosis value is almost constant. Consequently, this simulation can effectively illustrate ECFR is more sensitive to the periodic impulses.

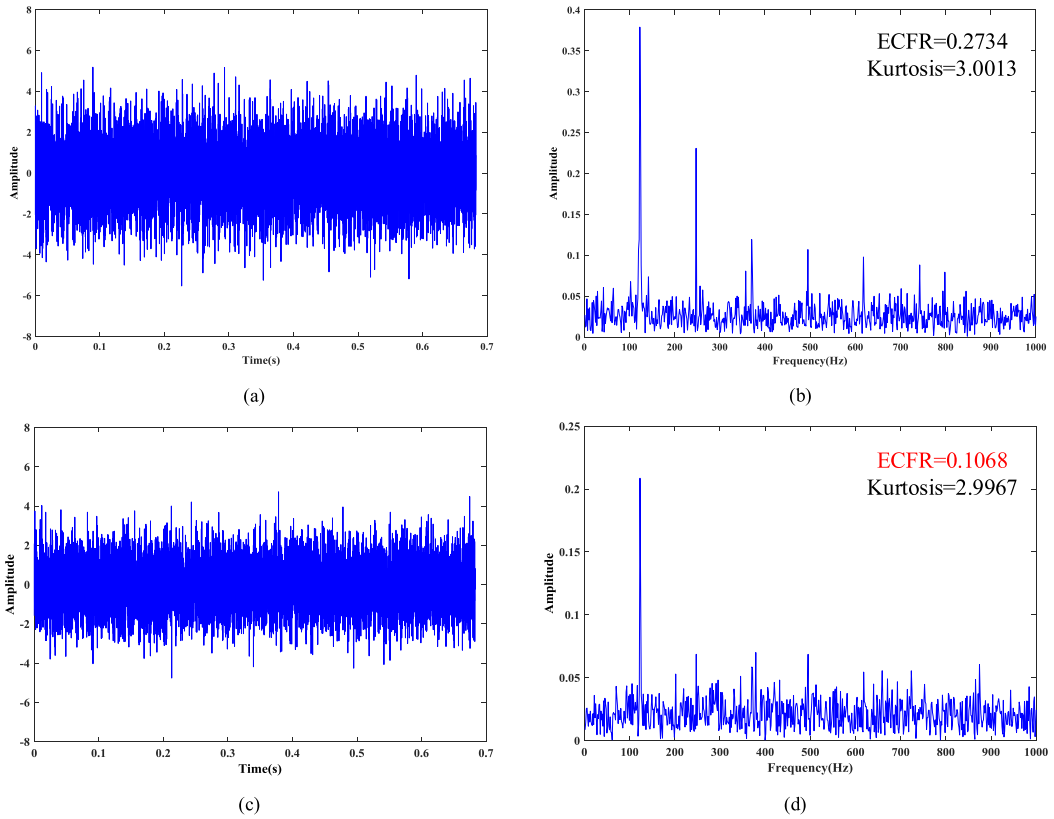

FIGURE 3. Sensitiveness to the periodic impulses: (a) The original simulation waveform with 1° random slippage of roller, (b) its envelope spectrum, (c) The original simulation waveform with 30° random slippage of roller, (d) its envelope spectrum.

3) ROBUSTNESS TO THE WEAK NOISE AND SUDDEN IMPULSES

Another simulation model is also conducted to illustrate ECFR is robust to the weak noise and sudden impulses. And the mathematical model can be expressed as (13):

$$y(t) = y_0 \exp(-\xi f_n t) \sin f_n \sqrt{1-\xi^2} t + n(t) \tag{13}$$

where $y(t)$ represents the simulated vibration signal, $y_0 = 5$ is the displacement constant, the natural frequency $f_n = 3000$Hz, damping coefficient $\xi = 0.1$, the outer race fault frequency $f_i = 233$Hz, and $n(t)$ denotes the WGN. Fig. 4 (a), (c), (d) displayed the original simulation waveform of bearing outer race fault which added the WGN with SNR =0dB, -1dB, and -2dB, respectively, and the waveform shown in Fig. 4 (b) is generated by adding a sudden impulse whose amplitude is 19m/s^2 on the basis of the waveform shown in (a). Through the comparative analysis among Fig. 4(a), (c) and (d), we can conclude that both ECFR and Kurtosis are robust enough to the weak noise, but the ECFR value is much more stable when the weak noise slowly increases. When a sudden impulse is added, as shown in Fig. 4 (b), ECFR is also almost constant, while the Kurtosis is sharply increased, that is to say, if a sudden shock appears on the test rig, Kurtosis index is highly possible to make a ridiculous selection of the optimal IMF components or even cause a false alarm for the condition monitoring of bearings.

In summary, two simulations fully prove that ECFR is an effective and stable criterion to select the optimal shape control parameter and further help to obtain the satisfactory decomposition results.

C. PARAMETER OPTIMIZATION USING GOA

After constructing the optimal parameter selection criterion, an excellent optimization algorithm is also very essential. GOA, which is newly proposed in 2017, is a superb optimization algorithm inspired by the grasshoppers swarming behavior in nature [35]. Compared with the conventional swarm intelligence algorithm, GOA has fewer adjustment parameters and higher convergence accuracy. In this algorithm, adult grasshoppers are responsible for exploring the entire global search space to obtain better food source areas, while the larval ones are responsible for exploiting an adjacent area of a particular location. The whole algorithm maintains a balance between the exploration of adult grasshoppers and the exploitation of larval ones, which gradually approximate the optimal solution. Finally, grasshoppers with the optimal fitness converge and approach the best solution. Actually, the position of grasshoppers X_i is affected by social interaction S_i, gravity force G_i and wind advection A_i. However, when solving the practical optimization problems, we need

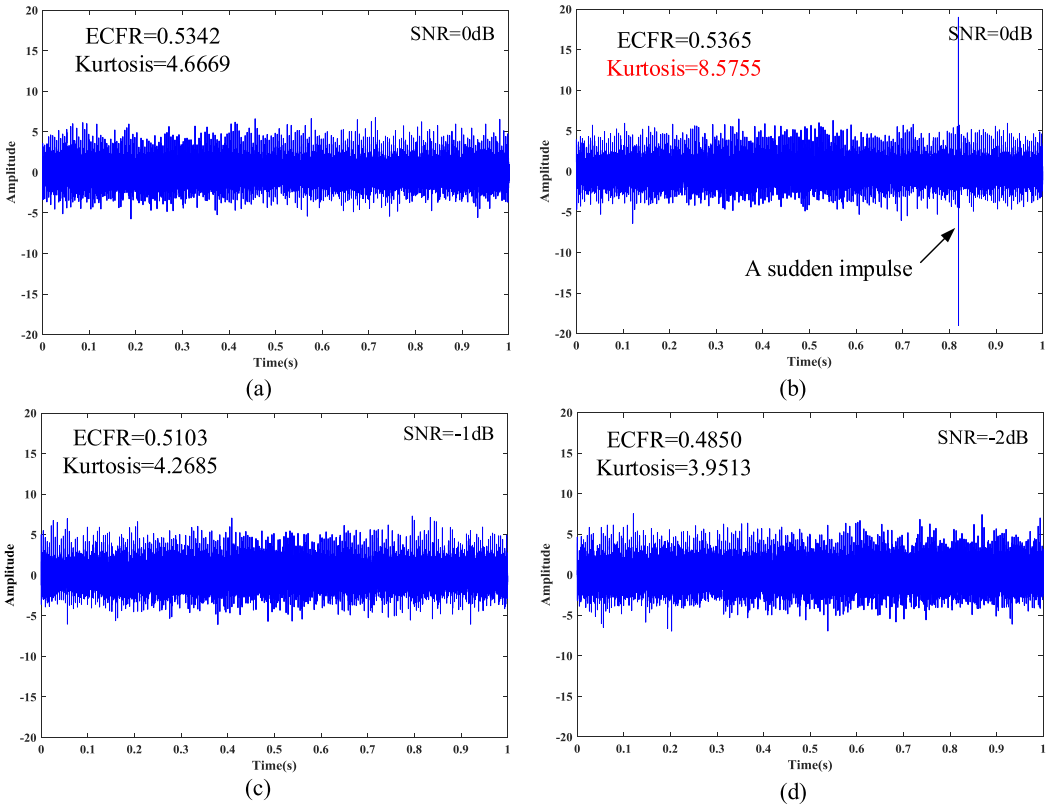

FIGURE 4. Robustness to the weak noise and sudden impulses: (a) The simulation waveform SNR = 0dB, (b) The simulation waveform SNR = 0dB with a sudden impulse, (c) The simulation waveform SNR = −1dB, (d) The simulation waveform SNR = −2dB.

to ignore the gravity effect and assume the wind direction in advance. Hence, the position of grasshoppers is updated according to (14) [35], [36]:

$$X_i^d = c\Big(\sum_{j=1,j\neq i}^{K} c\frac{ub_d - lb_d}{2} s\Big(\left|X_j^d - X_i^d\right|\Big)\frac{X_j - X_i}{d_{ij}}\Big) + \hat{T}_d \quad (14)$$

ub_d and lb_d represent the upper bounds and lower bounds, respectively, $d_{ij} = |x_i - x_j|$ means the distance between grasshoppers, K is the population size. $\hat{T}_d$ means the local optimal solution, $s(\cdot)$ denotes the function for calculating the social forces of grasshoppers, and its calculation formula is as follow:

$$s(r) = fe^{-r/l} - e^{-r} \quad (15)$$

f and l denote the strength of attraction and attractive length scale, respectively, and $f = 0.5$ and $l = 1.5$ are adopted in this paper.

c is mainly responsible for shrinking to the appropriate range in iteration process, c is updated as (16):

$$c = c\_\max - l\frac{c\_\max - c\_\min}{L} \quad (16)$$

From the above discussion, we can see that the advantage of GOA is that the updating of each individual location depends on the participation of all individuals in the whole optimization process, so as to improve the convergence accuracy.

The optimization process using GOA is summarized as follows. Firstly, initialize the population and related parameters; Secondly, evaluate the fitness of all current individuals and mark the best individual; Subsequently, update each individual's position according to (14), and determine whether the iteration number reaches the termination condition. Grasshopper individual moves in the direction of the optimal solution in each search process, and gradually approaches the global optimal solution.

D. THE PROPOSED I-EMD ALGORITHM

After constructing optimal parameter selection criterion and selecting the optimization method, the adaptive weighted rational quartic spline based EMD method is completely designed. And the objective function is expressed as the form of (17).

$$\begin{cases} fitness = \min\limits_{\gamma=(\alpha,\beta)} \{-ECFR\} \\ s.t.\ \alpha \in [1,5] \\ \quad\ \beta \in [1,5] \end{cases} \quad (17)$$

where *fitness* represents the objective function, and $\gamma = (\alpha, \beta)$ are the shape control parameters to be optimized. And in this paper, α, β takes the real number in

the interval of [1,5], respectively. The specific steps of the I-EMD algorithm can be concluded as follows:

1) Input the rolling bearing vibration signal, its dispersed sequence can be expressed as $X(j)(j = 1, 2 \ldots, N_s)$, N_s represents the data length of the vibration signal. Set the range of the shape control parameters α, β, calculate the fault characteristic frequencies and their harmonics. Subsequently, initialize the GOA parameters (Search agents $H = 30$, maximum iterations $I = 15$.

2) Construct the envelope curves of the vibration signal using the optimized weighted rational quartic spline interpolation with the initial parameter. And calculate the envelope mean $m(t)$, the difference $h(t)$ between $x(t)$ and $m(t)$. If $h(t)$ satisfies the IMF conditions [15], the first order component is preliminarily obtained.

3) Calculate the *fitness* of the first order components with each individual parameter in all agents and iterations. Then, the optimal component which has the minimum *fitness* is searched by GOA, and the first order improved IMF (I-IMF) $c_1(t)$ is obtained finally.

4) Repeat the steps 1)-3) until the decomposition stop criterion is satisfied [15], and the optimal I-IMFs $c_i(t)$ of the other orders are obtained successively.

Subsequently, a quantitative indicator termed weighted Kurtosis index (KCI) [36] which combines the advantages of Kurtosis and correlation coefficient is used to select the sensitive modes for further Hilbert envelope spectrum analysis in this paper. The calculation formula is expressed as (18)-(20).

$$Ku = \frac{\frac{1}{N_s}\sum_{j=1}^{N_s}(X(j)-\bar{X})^4}{[\frac{1}{N_s}\sum_{j=1}^{N_s}(X(j)-\bar{X})^2]^2} \tag{18}$$

$$C = \frac{\sum_{j=1}^{N_s}[c_i(j)-\bar{c}_i][X(j)-\bar{X}]}{\sqrt{\sum_{j=1}^{N_s}[c_i(j)-\bar{c}_i]^2\sum_{j=1}^{N_s}[X(j)-\bar{X}]^2}} \tag{19}$$

$$KCI = Ku \cdot |C| \tag{20}$$

where Ku represents the Kurtosis index of the specific mode, C denotes the correlation coefficient between the *ith* I-IMF mode $c_i(t)$ and raw vibration signal $X(t)$, and $c_i(j)$, $X(j)$ are their dispersed sequence, $\bar{c}_i$, $\bar{X}$ represent their sample mean, respectively. KCI means the weighted Kurtosis index. A larger KCI value denotes better impact characteristics which also implies a more sensitive mode with abundant fault feature information [36].

The flowchart of I-EMD algorithm is presented in Fig. 5.

IV. CASE VALIDATION

In this section, two cases on bearing fault diagnosis with different failure categories using different test devices are implemented to verify the proposed method. Furthermore, the comparative analysis with other popular signal processing methods (i.e. the conventional EMD, VMD and CEEMDAN) highlight the superiority of the I-EMD method.

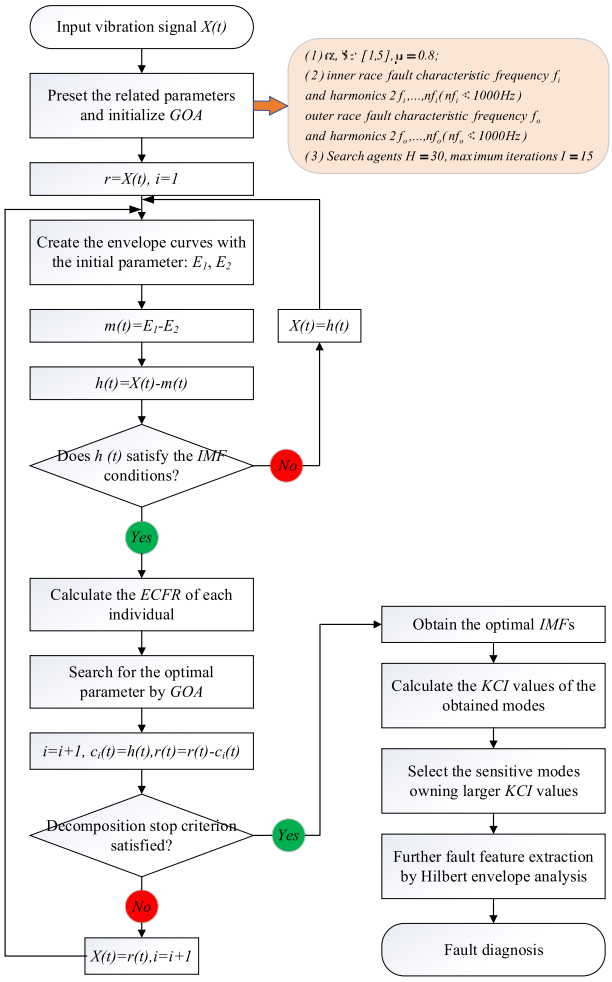

FIGURE 5. The flowchart of I-EMD algorithm.

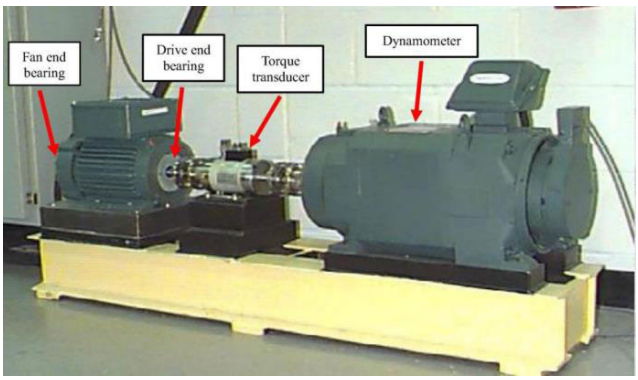

FIGURE 6. The test device of CWRU.

A. CASE 1: BEARING INNER RACE FAULT DIAGNOSIS USING CWRU DATA

The vibration signal is collected from the Bearing Data Center of CWRU [38], [39], which is especially popular for verification of new method in fault diagnosis. Fig. 6 displayed

TABLE 1. The related information of the experiment in case 1.

Fault category	Inner race fault
Fault diameter	0.014mm
Fault characteristic frequency	155.3Hz
Shaft speed	1728rpm
Rotational frequency	28.8Hz
Sampling frequency	12kHz
Data points	6000

the experimental rig, for a detailed description of the entire test and data, please refer to [38], [39]. This case only focuses on the bearing with inner race fault and its vibration signals, the related information are illustrated in Table 1. Although this data base is pretty pure and ideal, it is still really perfect for verifying the method presented in this paper.

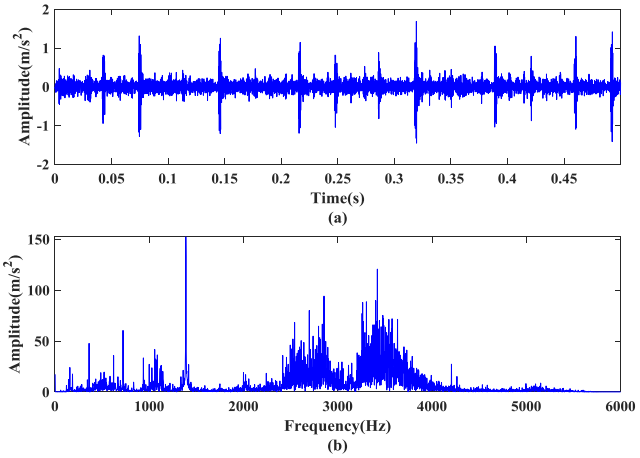

FIGURE 7. The original vibration signal in case 1: (a) Time-domain waveform, (b) frequency-domain spectrum.

1) SIGNAL PROCESSING-BASED FAULT DIAGNOSIS USING I-EMD METHOD

Time-domain graphic and its FFT spectrum of the studied vibration signal is displayed in Fig. 7, and no obvious and definite characteristic information can be clearly identified due to the existence of interference components.

Firstly, operate I-EMD on the raw vibration signal, and the decomposition results of the first five I-IMF are displayed in Fig. 8. Obviously, there is no mode mixing in these obtained components.

And the quantitative measurement index KCI of the first five modes are also calculated and marked in Fig. 8, and the first three I-IMF components which have the larger KCI values are considered as the sensitive I-IMFs for further fault feature extraction by Hilbert envelope spectrum, which is displayed in Fig. 9.

From the result in Fig. 9, the rotation frequency f_r, the inner race fault characteristic frequency f_i and harmonics frequencies ($2f_i$, $3f_i$, $4f_i$, $5f_i$) can be clearly extracted from the mode I-IMF1. Moreover, due to the modulation and demodulation

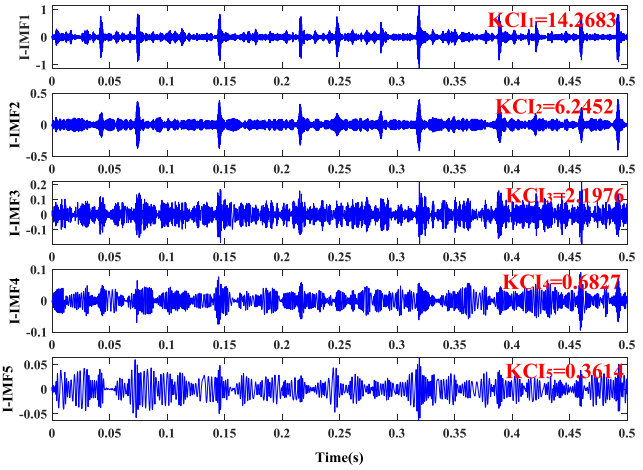

FIGURE 8. The first five I-IMF components generated by I-EMD method in case 1.

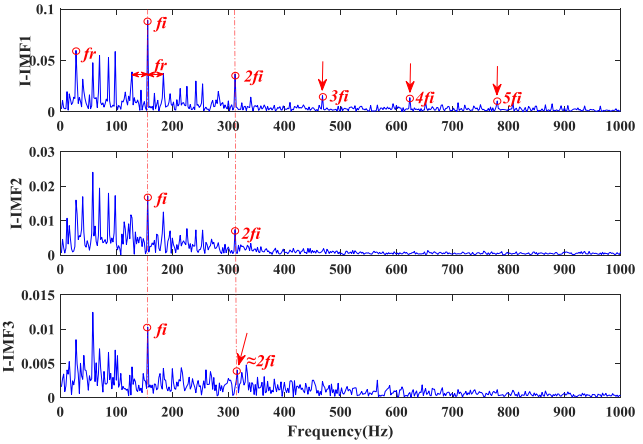

FIGURE 9. The Hilbert envelope spectrum of the sensitive I-IMF components in case 1.

effect, $f_i + f_r$ and $f_i - f_r$ can also be identified, which indicates the serious local inner race defect has occurred. Meanwhile, the fault feature frequency information can also be observed in the second and third I-IMF mode. In addition, we can conclude that the larger the KCI is, the more definite and obvious information can be observed in the corresponding mode, which indicates that the sensitive mode section criterion is feasible. The above analysis can fully prove the effectiveness and rationality of I-EMD in fault feature extraction.

2) COMPARATIVE ANALYSIS WITH OTHER METHODS

In this subsection, the conventional EMD, VMD and CEEMDAN are also presented for comparison using the same signal.

a: COMPARISONS WITH THE CONVENTIONAL EMD

The decomposition results and Hilbert envelope spectra of sensitive modes are displayed in Fig. 10 and Fig. 11.

We can see that the mode mixing phenomenon appears in the fifth IMFcomponents which is denoted by the red rectangles, while this phenomenon has been restrained apparently by I-EMD method as shown in Fig. 8. As displayed in Fig. 11,

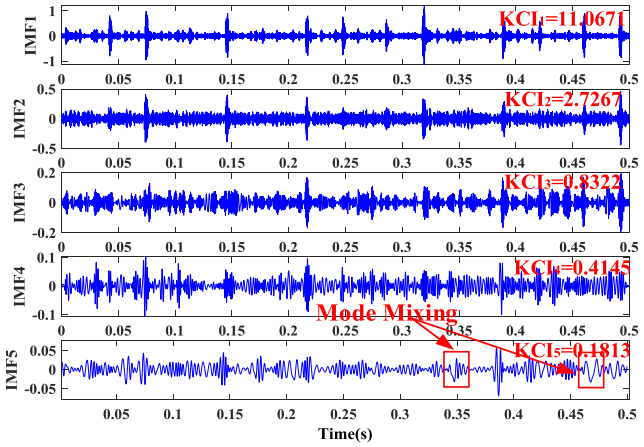

FIGURE 10. The first five IMF components generated by EMD method in case 1.

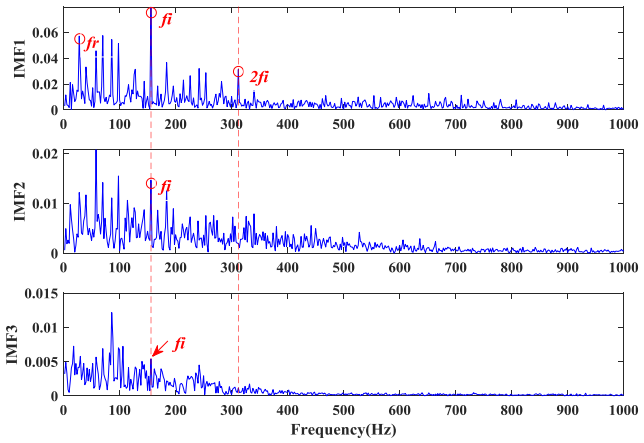

FIGURE 11. The Hilbert envelope spectrum of the sensitive IMF components of EMD in case 1.

the rotation frequency f_r and the characteristic frequency f_i can be observed in IMF1, but the f_i has already been very weak in IMF2, which is hard to be identified. Meanwhile, the fault feature information is nearly submerged by other interference frequency components in IMF3. Hence, we can conclude that when the fault feature itself is relatively faint, the conventional EMD may not be possible to provide more valuable information for accurate fault diagnosis.

Furthermore, a section of 120 data points from raw signal are intercepted, we also construct the envelope curves in the first-order sifting process by weighted rational quartic spline interpolation proposed in this paper ($\alpha = 1.23$, $\beta = 1.87$ are obtained by optimization using GOA) and conventional cubic spline interpolation to further explain the above comparison results. From Fig. 12, we can see that the weighted rational quartic spline-based envelope curve is more tense and accurate, which effectively restrains the over and undershoot problems. Since a smaller bandwidth indicates more concentrated signal energy and closer scale characteristics, 3dB bandwidth index is also employed to further evaluate the performance of envelope spline as well as the alleviation degree of mode mixing. And the calculation results are shown

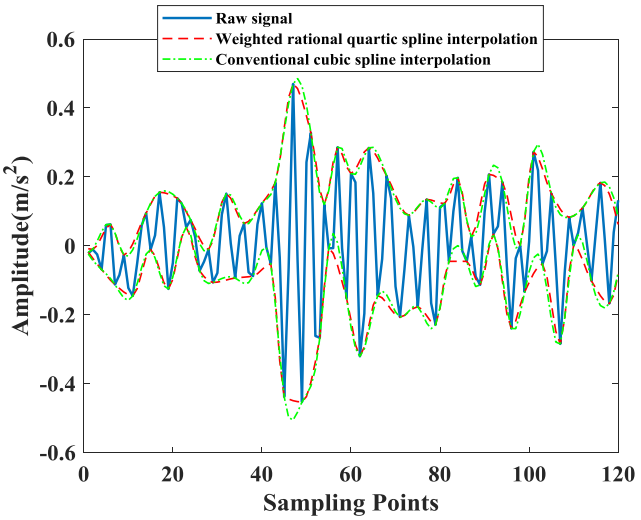

FIGURE 12. Envelope curves in the sifting process by weighted rational quartic spline interpolation and cubic spline interpolation in case 1.

TABLE 2. The calculation results of 3dB bandwidth index in case 1.

	IMF1	IMF2	IMF3	IMF4	IMF5
I-EMD	281Hz	233Hz	293Hz	147Hz	73Hz
EMD	317Hz	779Hz	653Hz	367Hz	229Hz

in Table 2. Obviously, the IMFs generated by I-EMD perform better properties than EMD. Consequently, these comparisons also fully illustrates the superiority of I-EMD and its exact reason.

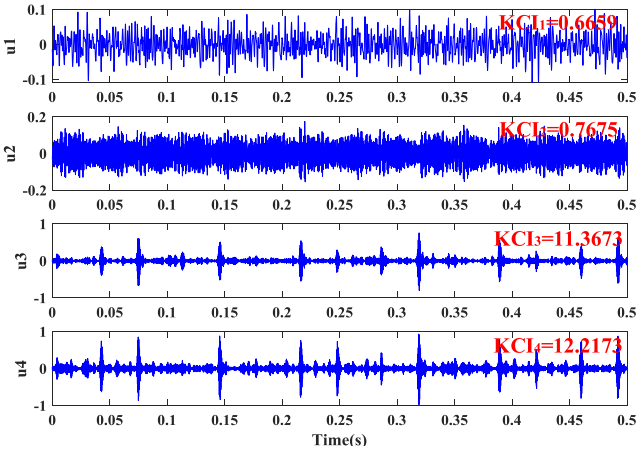

FIGURE 13. The components generated by VMD method in case 1.

b: COMPARISONS WITH VMD

In this case, $K = 4$ and $\alpha = 2000$ in VMD are adopted by analyzing the distribution of the center frequency in each mode [40]. The decomposition modes and its Hilbert envelope spectra are displayed in Fig. 13, 14 respectively. Because of the unique advantages of VMD, there is no mode mixing phenomenon appears. Although the characteristic frequency f_i and $2f_i$ can be identified in u_3 and u_4, there is nearly

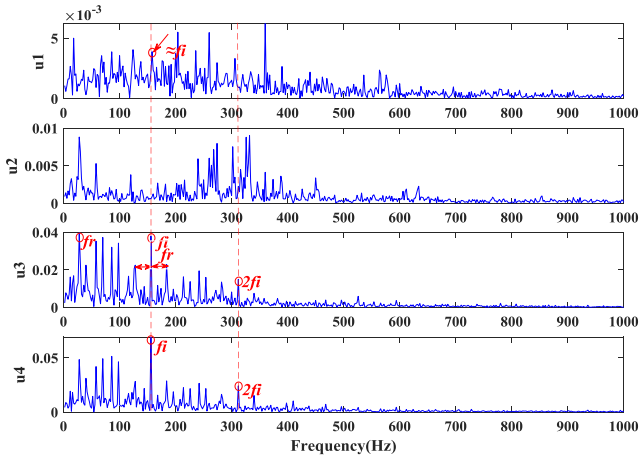

FIGURE 14. The Hilbert envelope spectrum of the obtained components of VMD in case *1*.

no useful fault-related information in the mode u_1 and u_2. Meanwhile, $3f_i$, $4f_i$, $5f_i$ which clearly appear in Fig. 9 can't be identified here.

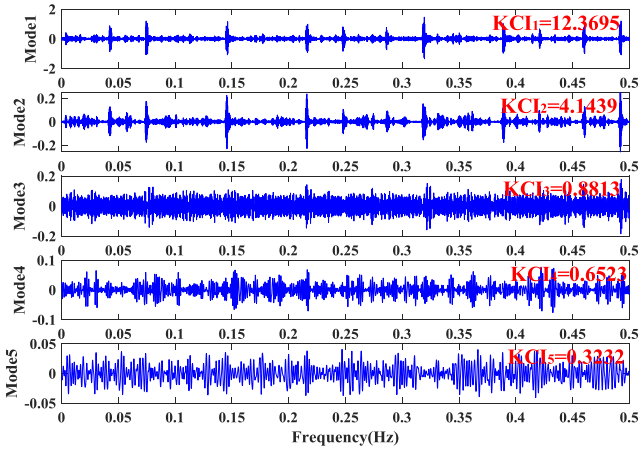

FIGURE 15. The first five I-IMF components generated by CEEMDAN method in case 1.

c: COMPARISONS WITH CEEMDAN

As an excellent and classical improved EMD method, CEEMDAN is also employed to decompose the same signal for comparison. The decomposition results and its Hilbert envelope spectra of sensitive modes are displayed in Fig. 15, 16. From Fig. 15, it can be concluded that CEEMDAN can restrain the mode mixing phenomenon effectively, but in the fault feature extraction aspect, although the characteristic frequency f_i and its harmonics frequencies are visible in the first mode, there is little useful defect information in the second and third mode compared with I-EMD method, moreover, the amplitude of fault characteristic frequency of CEEMDAN is also much smaller.

In addition, two indices (i.e. envelope entropy [41] and ECFR presented in this paper) of the reconstructed signal are also employed to quantitatively evaluate the decomposition

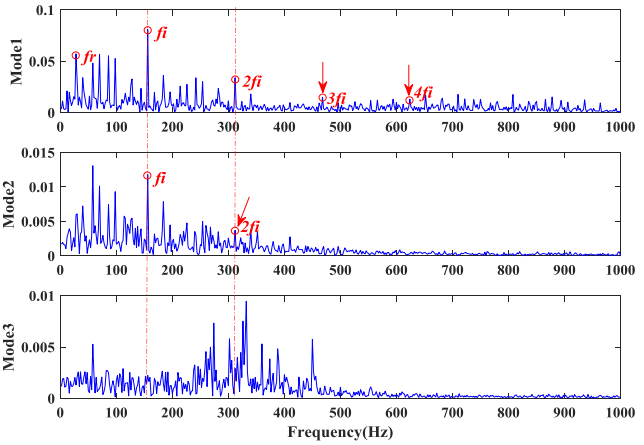

FIGURE 16. The Hilbert envelope spectrum of the sensitive modes of CEEMDAN in case 1.

performance and quality of these signal processing methods from the aspects of sparsity and impact properties.

The calculation of envelope entropy is expressed as (21), and the signal owning strong sparsity will have a smaller envelope entropy value. In contrast, if there are more noises and interference components, the envelope entropy value will be larger.

$$E_p = -\sum_{j=1}^{N_p} P_j \lg P_j$$
$$P_j = a(j)/\sum_{j=1}^{N_p} a(j) \tag{21}$$

where E_p means the envelope entropy value, P_j is the normalized form of $a(j)$, and $a(j)$ is the demodulated envelope signal of $X(j)$.

ECFR value can be directly used to reflect the capability of fault feature extraction. The definition and calculation of ECFR have been presented in Section III. And the calculation results of two indices are shown in Fig. 17.

From Fig. 17, we can see that the reconstructed signal by I-EMD method owns the smallest envelope entropy value as well as the largest ECFR value, which implies a better sparsity and impact property. So this quantitative comparison can also further highlight the decomposition performance of I-EMD method.

Consequently, this case fully demonstrates that I-EMD effectively improve the envelope curve and restrain the mode mixing phenomenon. Meanwhile, it also outperforms in fault feature extraction under the same conditions, and these comparisons also highlight its superiority in signal processing.

B. CASE 2: BEARING OUTER RACE FAULT DIAGNOSIS USING NASA DATA

In this subsection, another test data collected from IMS [42] is also used to verify the I-EMD method as a exclusion of occasionality. The experimental rig is depicted in Fig. 18, this case only focuses on the Bearing 1 which eventually fails

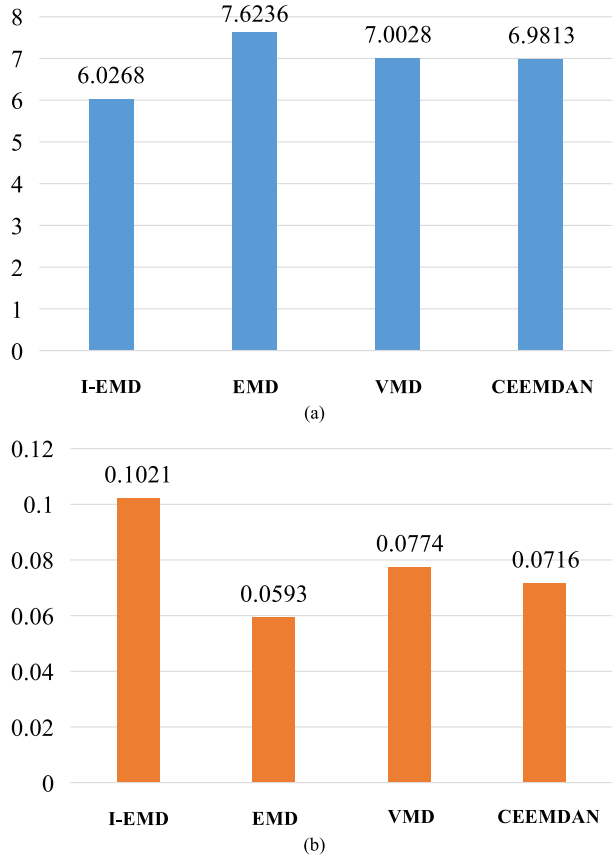

FIGURE 17. Quantitative evaluation of signal processing methods in case 1. (a) The envelope entropy value. (b) The ECFR value.

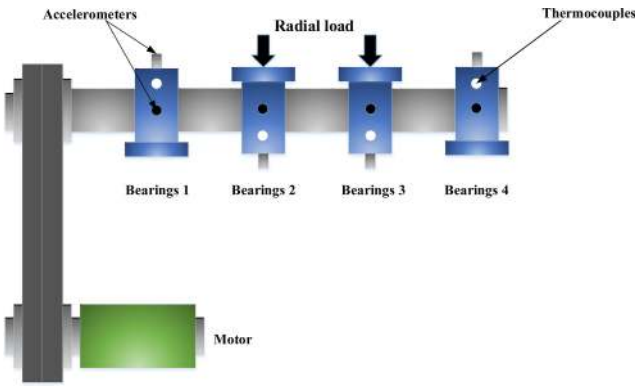

FIGURE 18. The experimental rig of IMS.

due to the outer race fault. Since this is a run to failure test, the fault feature in each stage are pretty ambiguous, whose incipient fault feature extraction is very suitable for verifying the I-EMD method in this paper. The related parameters information is illustrated in Table 3.

1) SIGNAL PROCESSING-BASED FAULT DIAGNOSIS USING I-EMD METHOD

Fig. 19 displays the time-domain graphic and its FFT spectrum of the raw vibration signal in the incipient fault stage.

TABLE 3. The related information in case 2.

Fault category	Fault characteristic frequency	Rotational speed	Radial load	Sampling frequency	Data points
Outer race fault	231Hz	2000rpm	6000lb	20kHz	6000

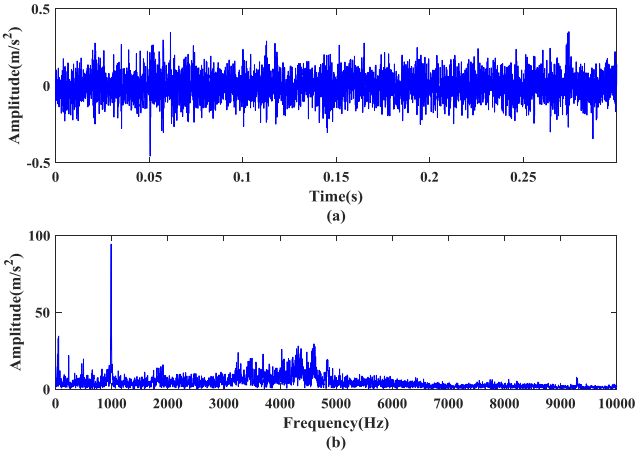

FIGURE 19. The original vibration signal in case 2: (a) Time-domain waveform, (b) Frequency-domain spectrum.

It is hard to extract more useful fault information because of the noises and other interference.

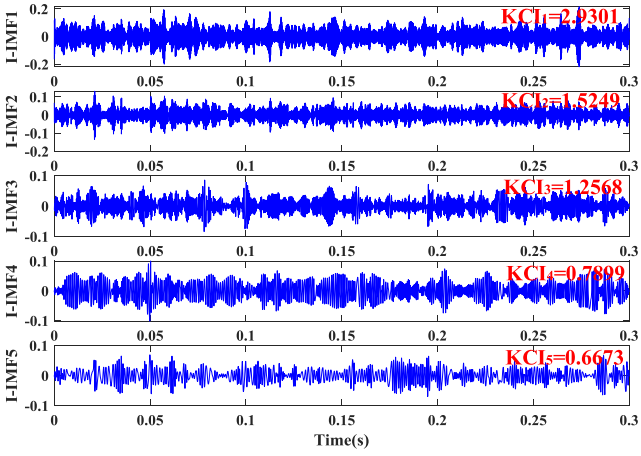

FIGURE 20. The first five I-IMF components generated by I-EMD method in case 2.

Similarly, the vibration signal is also firstly decomposed and analyzed by I-EMD method. And the first five I-IMF components are presented in Fig. 20, meanwhile, the KCI values are also calculated and marked in Fig. 20 to select the sensitive modes.

Subsequently, the first three I-IMF components which have larger KCI values are selected for further Hilbert envelope analysis, as shown in Fig. 21. From this figure, the outer race fault characteristic frequency f_o and its harmonic frequencies

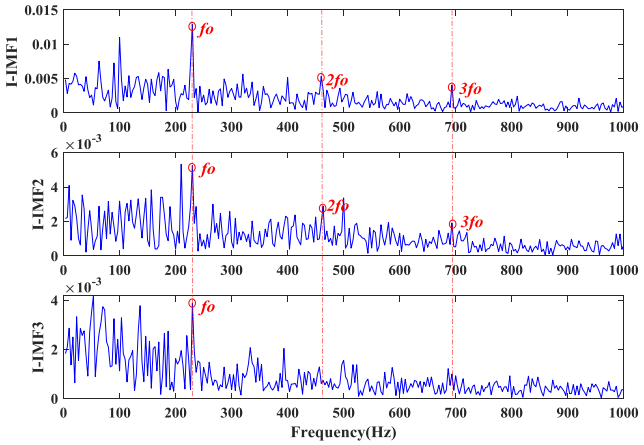

FIGURE 21. The Hilbert envelope spectrum of the sensitive I-IMF components in case 2.

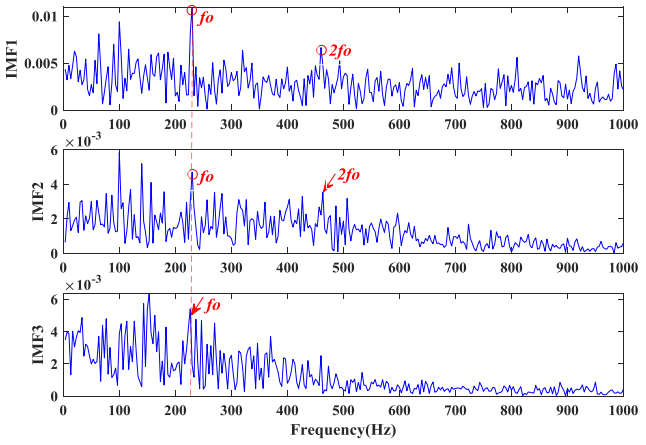

FIGURE 23. The Hilbert envelope spectrum of the sensitive IMF components of EMD in case 2.

($2f_o$, $3f_o$) are obviously identified in the first and the second I-IMF. Meanwhile, f_o can also be observed in the third mode, which proves that the I-EMD is able to extract more abundant fault feature.

2) COMPARATIVE ANALYSIS WITH OTHER METHODS

The conventional EMD, VMD and CEEMDAN are also used for comparison in this case.

a: COMPARISONS WITH THE CONVENTIONAL EMD

The decomposition results of EMD and its corresponding Hilbert envelope spectra of sensitive modes are shown in Fig. 22 and Fig. 23.

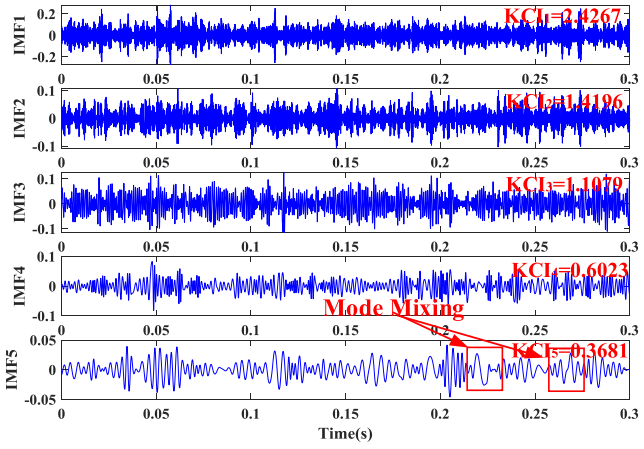

FIGURE 22. The first five IMF components generated by EMD method in case 2.

From Fig. 22, the mode mixing phenomenon (denoted by red rectangles) appears in the fifth IMF mode, which is restrained effectively by I-EMD in Fig. 20.

The Hilbert envelope spectra in Fig. 23 illustrate that although the characteristic frequency f_o can be identified in the first IMF mode, the fault information is nearly buried by other interference frequency components in the second and third IMF. Hence, if there are more interference components in the original vibration signal, fewer fault information will be provided, which significantly limits the accuracy of fault diagnosis.

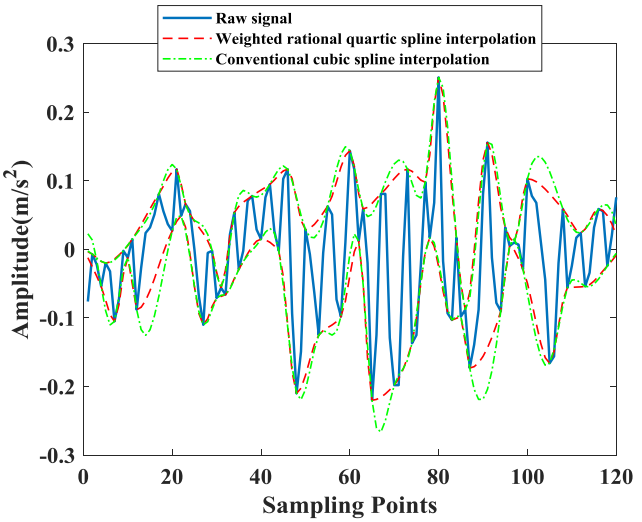

FIGURE 24. Envelope curves in the sifting process by weighted rational quartic spline interpolation and cubic spline interpolation in case 2.

TABLE 4. The calculation results of 3dB bandwidth index in case 2.

	IMF1	IMF2	IMF3	IMF4	IMF5
I-EMD	1012Hz	1083Hz	235Hz	281Hz	177Hz
EMD	1178Hz	1446Hz	419Hz	652Hz	239Hz

Furthermore, a section of 120 data points from raw signal are intercepted, we also construct the envelope curves in the first-order sifting process for comparison. From Fig. 24, we can see that the weighted rational quartic spline based envelope curve ($\alpha = 2.138$, $\beta = 2.793$ are obtained by the optimization using GOA) is more tense and accurate, which

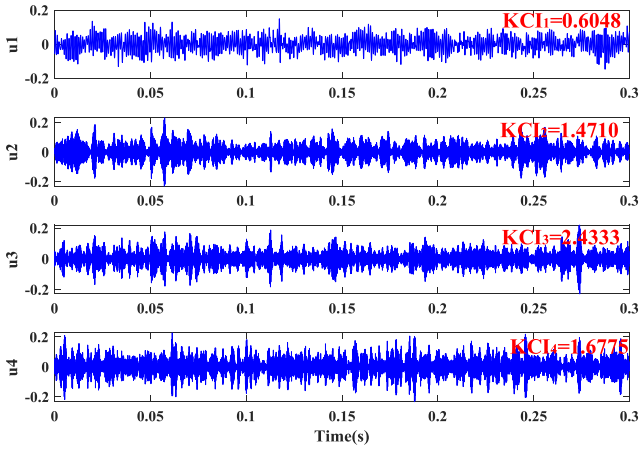

FIGURE 25. The components generated by VMD method in case 2.

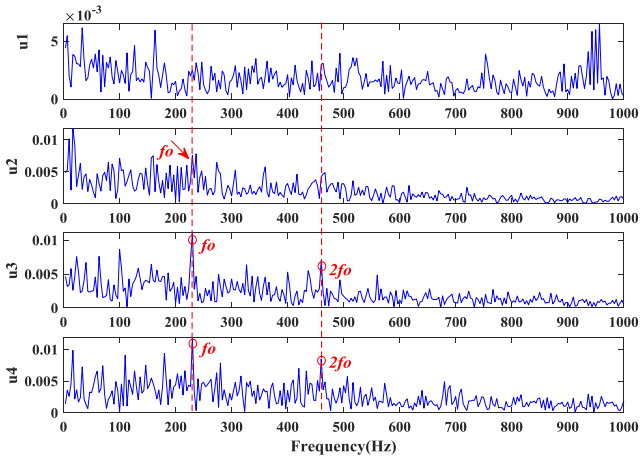

FIGURE 26. The Hilbert envelope spectrum of the obtained components of VMD in case 2.

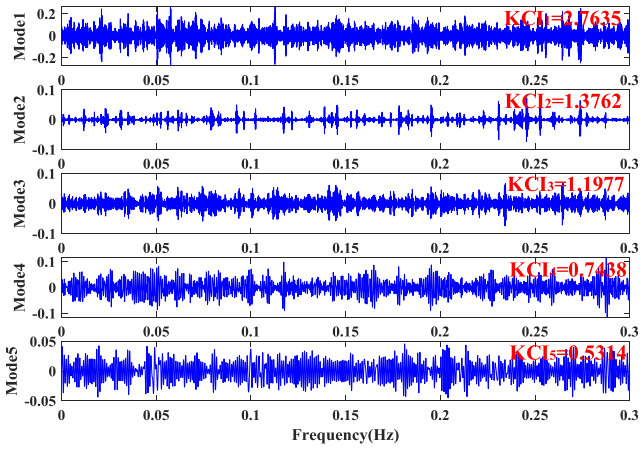

FIGURE 27. The first five I-IMF components generated by CEEMDAN method in case 2.

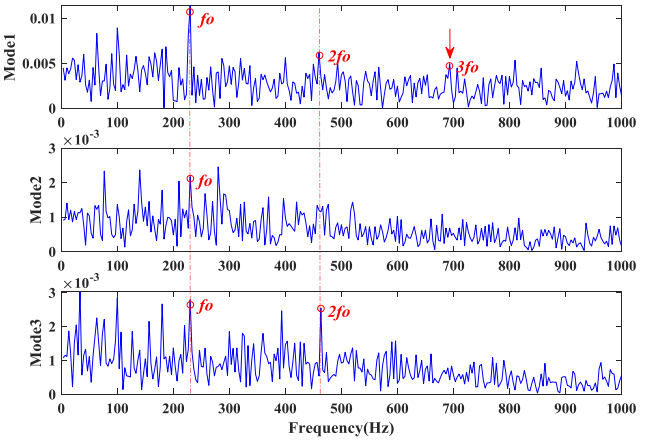

FIGURE 28. The Hilbert envelope spectrum of the sensitive modes of CEEMDAN in case 2.

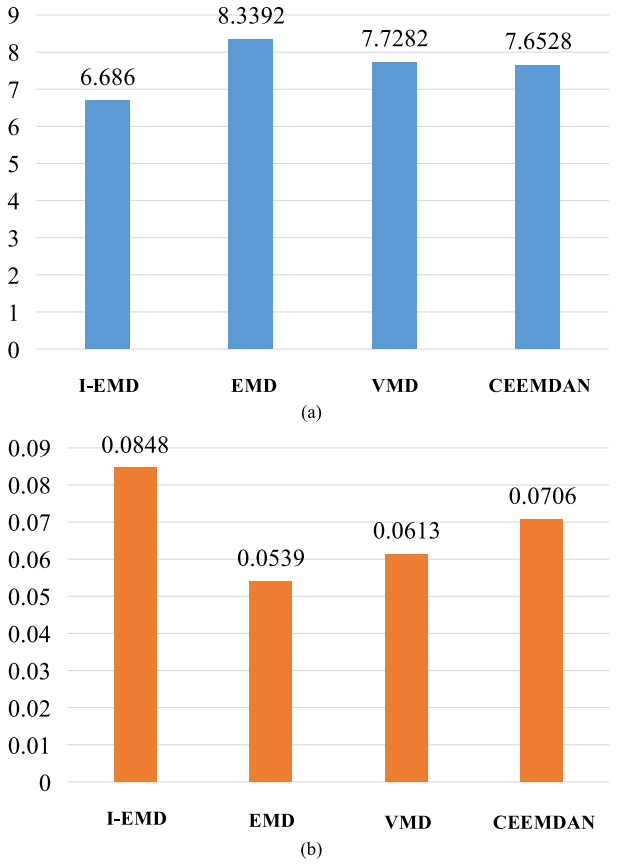

FIGURE 29. Quantitative evaluation of signal processing methods in case 2. (a) The envelope entropy value. (b) The ECFR value.

evidently restrains the over and undershoot problems. 3dB bandwidth index is also calculated to further evaluate the performance of envelope spline as well as the alleviation degree of mode mixing, which is shown in Table 4. Consequently, these comparisons also directly illustrate the exact reason of the superiority of I-EMD and definitely explain the above comparison results.

b: COMPARISONS WITH VMD

$K = 4$ and $\alpha = 2000$ are taken in VMD method. The obtained modes and the corresponding Hilbert envelope spectra are presented in Fig. 25 and Fig. 26. The characteristic frequency f_o and $2f_o$ can be observed in Fig. 26, but the

harmonic frequency $3f_o$ which clearly appears in Fig. 21 can't be identified here.

c: COMPARISONS WITH CEEMDAN

CEEMDAN is also employed to analyze the NASA data for comparison. And the decomposition modes and Hilbert envelope spectra of sensitive modes are also displayed in Fig. 27 and Fig. 28. From this figure, although CEEMDAN can alleviate the mode mixing phenomenon compared with the conventional EMD method, but it performs more modestly in extracting defect information than I-EMD method shown in Fig. 21, and the amplitude of fault characteristic frequency of the second and third mode is also much smaller.

Subsequently, the envelope entropy and ECFR are also employed to evaluate the decomposition performance of these signal processing methods in this case, the calculation results of the two indices are shown in Fig. 29. The outcome also displayed that I-EMD performs best among these mentioned signal processing methods.

In summary, two cases on bearing fault diagnosis with different failure categories using different test devices fully demonstrate the effectiveness of the I-EMD in constructing the envelope curves, alleviating the mode mixing and extracting more abundant fault features, and the corresponding comparative analysis further highlights its advantages and better performance.

V. CONCLUSION

In this paper, an improved EMD based on adaptive weighted rational quartic spline is proposed to achieve that each obtained mode is optimum throughout the whole sifting process adaptively. Two case studies combined with comparative analysis demonstrate that the I-EMD method can solve the over and undershoot problem in the sifting process and restrain the mode mixing phenomenon effectively. Moreover, I-EMD also has better capacity of fault feature extraction through the qualitative and quantitative assessment, in particular, the envelope characteristic frequency ratio obtained by I-EMD is respectively improved by 72.18% and 57.33% in two cases compared with conventional EMD.

Some highlights and main contributions are further concluded: 1) A new interpolation method termed weighted rational quartic spline interpolation is designed in this paper to construct more flexible and accurate envelope curves, this may also provide a new idea for the improvement of similar methods, such as EEMD and LMD; 2) The novel parameter selection criterion termed ECFR is established to help to generate the optimal mode owning the most abundant fault feature information; 3) Simulation analysis proved that ECFR is not only sensitive to the periodic impulses but also robust to the weak noise and sudden impulses, so it is also likely to be employed as a promising fault feature or index for indicating the health condition of bearings.

In the future, some effective and adaptive band pass filter based EMD methods should be developed to locate the optimal band with abundant and explicit fault features for the incipient diagnosis of rotating machinery.

REFERENCES

[1] J. Wang, Z. Mo, H. Zhang, and Q. Miao, "A deep learning method for bearing fault diagnosis based on time-frequency image," *IEEE Access*, vol. 7, pp. 42373–42383, 2019.
[2] J. Li, M. Li, and J. Zhang, "Rolling bearing fault diagnosis based on time-delayed feedback monostable stochastic resonance and adaptive minimum entropy deconvolution," *J. Sound Vib.*, vol. 401, pp. 139–151, Aug. 2017.
[3] L. Meng, J. Xiang, Y. Wang, Y. Jiang, and H. Gao, "A hybrid fault diagnosis method using morphological filter-translation invariant wavelet and improved ensemble empirical mode decomposition," *Mech. Syst. Signal Process.*, vols. 50–51, pp. 101–115, Jan. 2015.
[4] J. Dybała and R. Zimroz, "Rolling bearing diagnosing method based on empirical mode decomposition of machine vibration signal," *Appl. Acoust.*, vol. 77, pp. 195–203, Mar. 2014.
[5] X. Zhang, Z. Liu, Q. Miao, and L. Wang, "An optimized time varying filtering based empirical mode decomposition method with grey wolf optimizer for machinery fault diagnosis," *J. Sound Vib.*, vol. 418, pp. 55–78, Mar. 2018.
[6] I. El-Thalji and E. Jantunen, "A summary of fault modelling and predictive health monitoring of rolling element bearings," *Mech. Syst. Signal Process.*, vols. 60–61, pp. 252–272, Aug. 2015.
[7] L. Wang, Z. Liu, Q. Miao, and X. Zhang, "Time-frequency analysis based on ensemble local mean decomposition and fast kurtogram for rotating machinery fault diagnosis," *Mech. Syst. Signal Process.*, vol. 103, pp. 60–75, Mar. 2018.
[8] L. Wang, Z. Liu, Q. Miao, and X. Zhang, "Complete ensemble local mean decomposition with adaptive noise and its application to fault diagnosis for rolling bearings," *Mech. Syst. Signal Process.*, vol. 106, pp. 24–39, Jun. 2018.
[9] D. Wang, K.-L. Tsui, and Q. Miao, "Prognostics and health management: A review of vibration based bearing and gear health indicators," *IEEE Access*, vol. 6, pp. 665–676, 2018.
[10] R. Rubini and U. Meneghetti, "Application of the envelope and wavelet transform analyses for the diagnosis of incipient faults in ball bearings," *Mech. Syst. Signal Process.*, vol. 15, no. 2, pp. 287–302, Mar. 2001.
[11] K. I. Rodopoulos and I. A. Antoniadis, "Instantaneous fault frequencies estimation in roller bearings via wavelet structures," *J. Sound Vib.*, vol. 383, pp. 446–463, Nov. 2016.
[12] Y. Pan, J. Chen, and X. Li, "Bearing performance degradation assessment based on lifting wavelet packet decomposition and fuzzy C-means," *Mech. Syst. Signal Process.*, vol. 24, no. 2, pp. 559–566, Feb. 2010.
[13] E.-Y. Kim, Y.-J. Lee, and S.-K. Lee, "Heath monitoring of a glass transfer robot in the mass production line of liquid crystal display using abnormal operating sounds based on wavelet packet transform and artificial neural network," *J. Sound Vib.*, vol. 331, no. 14, pp. 3412–3427, Jul. 2012.
[14] Z. Liu, Z. He, W. Guo, and Z. Tang, "A hybrid fault diagnosis method based on second generation wavelet de-noising and local mean decomposition for rotating machinery," *ISA Trans.*, vol. 61, pp. 211–220, Mar. 2016.
[15] N. E. Huang, Z. Shen, S. R. Long, M. C. Wu, H. H. Shih, Q. Zheng, N.-C. Yen, C. C. Tung, and H. H. Liu, "The empirical mode decomposition and the Hilbert spectrum for nonlinear and non-stationary time series analysis," *Proc. Roy. Soc. London. A, Math., Phys. Eng. Sci.*, vol. 454, no. 1971, pp. 903–995, Mar. 1998.
[16] J. Gai and Y. Hu, "Research on fault diagnosis based on singular value decomposition and fuzzy neural network," *Shock Vib.*, vol. 2018, pp. 1–7, Jan. 2018.
[17] J. Ben Ali, N. Fnaiech, L. Saidi, B. Chebel-Morello, and F. Fnaiech, "Application of empirical mode decomposition and artificial neural network for automatic bearing fault diagnosis based on vibration signals," *Appl. Acoust.*, vol. 89, pp. 16–27, Mar. 2015.
[18] N. E. Huang and Z. Wu, "A review on Hilbert-Huang transform: Method and its applications to geophysical studies," *Rev. Geophys.*, vol. 46, no. 2, pp. 1–23, Jun. 2008.
[19] J. Xiang and Y. Zhong, "A fault detection strategy using the enhancement ensemble empirical mode decomposition and random decrement technique," *Microelectron. Rel.*, vol. 75, pp. 317–326, Aug. 2017.
[20] J. Yang, D. Huang, D. Zhou, and H. Liu, "Optimal IMF selection and unknown fault feature extraction for rolling bearings with different defect modes," *Measurement*, vol. 157, Jun. 2020, Art. no. 107660.

[21] Y. Cheng, Z. Wang, B. Chen, W. Zhang, and G. Huang, "An improved complementary ensemble empirical mode decomposition with adaptive noise and its application to rolling element bearing fault diagnosis," *ISA Trans.*, vol. 91, pp. 218–234, Aug. 2019.

[22] A. Kumar, C. P. Gandhi, Y. Zhou, R. Kumar, and J. Xiang, "Variational mode decomposition based symmetric single valued neutrosophic cross entropy measure for the identification of bearing defects in a centrifugal pump," *Appl. Acoust.*, vol. 165, Aug. 2020, Art. no. 107294.

[23] R. Gu, J. Chen, R. Hong, H. Wang, and W. Wu, "Incipient fault diagnosis of rolling bearings based on adaptive variational mode decomposition and Teager energy operator," *Measurement*, vol. 149, Jan. 2020, Art. no. 106941.

[24] H. Liu and J. Xiang, "A strategy using variational mode decomposition, L-Kurtosis and minimum entropy deconvolution to detect mechanical faults," *IEEE Access*, vol. 7, pp. 70564–70573, 2019.

[25] D. Zhao, Z. Huang, H. Li, J. Chen, and P. Wang, "An improved EEMD method based on the adjustable cubic trigonometric cardinal spline interpolation," *Digit. Signal Process.*, vol. 64, pp. 41–48, May 2017.

[26] A. Bouchikhi and A.-O. Boudraa, "Multicomponent AM-FM signals analysis based on EMD-B-splines ESA," *Signal Process.*, vol. 92, no. 9, pp. 2214–2228, Sep. 2012.

[27] S. Xia, J. Zhang, S. Ye, B. Xu, J. Xiang, and H. Tang, "A mechanical fault detection strategy based on the doubly iterative empirical mode decomposition," *Appl. Acoust.*, vol. 155, pp. 346–357, Dec. 2019.

[28] S. D. Hawley, L. E. Atlas, and H. J. Chizeck, "Some properties of an empirical mode type signal decomposition algorithm," *IEEE Signal Process. Lett.*, vol. 17, no. 1, pp. 24–27, Jan. 2010.

[29] Q. H. Chen, N. Huang, S. Riemenschneider, and Y. S. Xu, "A B-spline approach for empirical mode decompositions," *Adv. Comput. Math.*, vol. 29, no. 1, p. 93, Jul. 2008.

[30] W. Zhu, H. Zhao, and X. Chen, "Improving empirical mode decomposition with an optimized piecewise cubic Hermite interpolation method," in *Proc. Int. Conf. Syst. Informat. (ICSAI)*, May 2012, pp. 1698–1701.

[31] H. Li, X. Qin, D. Zhao, J. Chen, and P. Wang, "An improved empirical mode decomposition method based on the cubic trigonometric B-spline interpolation algorithm," *Appl. Math. Comput.*, vol. 332, pp. 406–419, Sep. 2018.

[32] Y. Li, M. Xu, Y. Wei, and W. Huang, "An improvement EMD method based on the optimized rational Hermite interpolation approach and its application to gear fault diagnosis," *Measurement*, vol. 63, pp. 330–345, Mar. 2015.

[33] T. Guo and Z. Deng, "An improved EMD method based on the multi-objective optimization and its application to fault feature extraction of rolling bearing," *Appl. Acoust.*, vol. 127, pp. 46–62, Dec. 2017.

[34] J. Wang and Q. He, "Wavelet packet envelope manifold for fault diagnosis of rolling element bearings," *IEEE Trans. Instrum. Meas.*, vol. 65, no. 11, pp. 2515–2526, Nov. 2016.

[35] S. Saremi, S. Mirjalili, and A. Lewis, "Grasshopper optimisation algorithm: Theory and application," *Adv. Eng. Softw.*, vol. 105, pp. 30–47, Mar. 2017.

[36] X. Zhang, Q. Miao, H. Zhang, and L. Wang, "A parameter-adaptive VMD method based on grasshopper optimization algorithm to analyze vibration signals from rotating machinery," *Mech. Syst. Signal Process.*, vol. 108, pp. 58–72, Aug. 2018.

[37] Y. Li, X. Liang, M. Xu, and W. Huang, "Early fault feature extraction of rolling bearing based on ICD and tunable Q-factor wavelet transform," *Mech. Syst. Signal Process.*, vol. 86, pp. 204–223, Mar. 2017.

[38] K. A. Loparo. *Bearing Data Center*. Case Western Reserve University. Accessed: Oct. 9, 2018. [Online]. Available: http://csegroups.case.edu/bearingdatacenter/pages/download-data-file

[39] W. A. Smith and R. B. Randall, "Rolling element bearing diagnostics using the case western reserve university data: A benchmark study," *Mech. Syst. Signal Process.*, vols. 64–65, pp. 100–131, Dec. 2015.

[40] M. Mishra, S. Banerjee, D. C. Thomas, S. Dutta, and A. Mukherjee, "Detection of third heart sound using variational mode decomposition," *IEEE Trans. Instrum. Meas.*, vol. 67, no. 7, pp. 1713–1721, Jul. 2018.

[41] H. Liu and M. Han, "A fault diagnosis method based on local mean decomposition and multi-scale entropy for roller bearings," *Mechanism Mach. Theory*, vol. 75, pp. 67–78, May 2014.

[42] J. Lee, H. Qiu, and G. Yu. *NASA Ames Prognostics Data Repository-Bearing Data Set*. Accessed: 2007. [Online]. Available: https://ti.arc.nasa.gov/tech/dash/groups/pcoe/prognostic-data-repository/

XUERONG YE (Senior Member, IEEE) received the B.S., M.S., and Ph.D. degrees in electrical engineering from the Harbin Institute of Technology, Harbin, China, in 2003, 2005, and 2009, respectively.

He is currently a Professor with the Department of Electrical Engineering, Harbin Institute of Technology. He has published more than 20 peer-reviewed journal articles. His research interests include the failure analysis, reliability design, and fault diagnosis of mechanical and electronic devices.

YIFAN HU was born in 1994. He received the B.S. and M.S. degrees from the College of Aerospace and Civil Engineering, Harbin Engineering University, Harbin, China, in 2016 and 2019, respectively. He is currently pursuing the Ph.D. degree with the School of Electrical Engineering and Automation, Harbin Institute of Technology, Harbin.

His current research interests include reliability analysis, fault diagnosis, prognostics, and health management.

JUNXIAN SHEN was born in 1995. He received the B.S. degree from the College of Aerospace and Civil Engineering, Harbin Engineering University, Harbin, China, in 2018, where he is currently pursuing the M.S. degree.

His current research interests include intelligent fault diagnosis of rotating machinery and adaptive signal processing techniques.

RUI FENG was born in 1996. He received the B.S. degree in electrical engineering from the Harbin Institute of Technology, Harbin, China, in 2018, where he is currently pursuing the M.S. degree in electrical engineering.

His research interests include reliability analysis and fault diagnosis of mechanical and electronic devices.

GUOFU ZHAI (Member, IEEE) received the Ph.D. degree in instrumentation science and technology from the Harbin Institute of Technology, Harbin, China, in 1998.

He is currently a Professor with the Department of Electrical Engineering, Harbin Institute of Technology. He has published more than 40 peer-reviewed journal articles. His research interests include reliability and testing techniques of mechanical and electronic devices and systems.